


## Field-triggered vertical positional transition of a microparticle suspended in a nematic liquid crystal cell

Ke Xiao, Xi Chen, Xue-Zheng Cao, and Chen-Xu Wu <sup>\*</sup>

*Department of Physics, School of Physical Science and Technology, Xiamen University, Xiamen 361005, People's Republic of China*



(Received 9 February 2020; accepted 11 May 2020; published 28 May 2020)

In this paper, based on the numerical calculation of total energy utilizing the Green's function method, we investigate how a field-triggered vertical positional transition of a microparticle suspended in a nematic liquid crystal cell is influenced by the direction of the applied field, surface anchoring feature, and nematic's dielectric properties. The new equilibrium position of the translational movement is decided via a competition between the buoyant force and the effective force built on the microparticle by the elastic energy gradient along the vertical direction. The threshold value of external field depends on thickness  $L$  and Frank elastic constant  $K$  and slightly on the microparticle size and density, in a Fréedericksz-like manner, but by a factor. For a nematic liquid crystal cell with planar surface alignment, a bistable equilibrium structure for the transition is found when the direction of the applied electric field is (a) perpendicular to the two plates of the cell with positive molecular dielectric anisotropy or (b) parallel to the two plates and the anchoring direction of the cell with negative molecular dielectric anisotropy. When the electric field applied is parallel to both plates and perpendicular to the anchoring direction, the microparticle suspended in the nematic liquid crystal tends to be trapped in the midplane, regardless of the sign of the molecular dielectric anisotropy. Such a phenomenon also occurs for negative molecular dielectric anisotropy if the external field is applied perpendicular to the two plates. Explicit formulas proposed for the critical electric field agree extremely well with the numerical calculation.

DOI: [10.1103/PhysRevE.101.052706](https://doi.org/10.1103/PhysRevE.101.052706)

### I. INTRODUCTION

Liquid crystals (LCs) are soft matter with anisotropic properties characterized by their long-range orientational order. In a nematic liquid crystal (NLC) phase, for example, molecules with molecular long axes possess a preferred orientation, which drives them to align along a common direction, while in a dispersed NLC, colloidal particles disturb the alignment of LC molecules, inducing elastic distortions which give rise to long-range anisotropic interactions and topological defects. Generally, there are three widely accepted and confirmed possible types of topological defect, namely hedgehog, Saturn-ring, and boojum defect [1–3]. Typically, the generated topological defects are usually determined by boundary conditions like surface anchoring features, particle size and shape, LC elasticity, and external fields, etc. [4–8]. In addition, very recently, the so-called elastic hexadecapole caused by the conically degenerated boundary condition [9] has been reported, and the dipole-hexadecapole transformation can be achieved via tuning the preferred tilt angle of LC molecules anchored on colloidal particle surface [10].

Since the early 2000s, the properties and behaviors of colloid-suspended NLC have attracted an increasing amount of interest and triggered a wide range of promising practical applications in new display and topological memory devices [11–13], new materials [14], report external triggers and release microcargo [15], and biological detectors [16,17].

Efforts using experiment, theoretical modeling, and computer simulation [4,18–29] have been devoted to getting a better understanding of the physics hidden behind colloidal particles embedded in an NLC cell. Experimentally, breakthroughs in versatile methods and techniques have enabled the measurement of the interaction force between particles in NLC in a direct manner [18,30–33]. It has been found that a number of factors, such as interparticle distance, geometrical confinement [19], and shape of particles [4], play a prime role in determining the pair interaction and aggregation of spherical particles suspended in NLC. In addition, fascinating physical phenomena such as levitation, lift, bidirectional motion, aggregation, and electrokinetic superdiffusion have been found for colloids dispersed in NLCs in the presence of an external electric field [29,34–36]. For example, the transition between elastic dipole and quadrupolar configuration, a phenomenon depending on particle size and surface anchoring strength [37–39], has been realized in experiments by applying an external field.

On the other hand, theoretical modeling and computer simulation provide a useful complement to experimental investigations. The system of colloidal particles dispersed in NLCs are typically modelled via Landau-de Gennes (LdG) theory and elastic free-energy method. Furthermore, Monte Carlo simulation [28,40], lattice Boltzmann method [41,42], and finite element method [19,43–46] are commonly adopted to minimize the LdG free-energy functional. Except for the methods mentioned above, recently the method of Green's function has been proposed to study the interaction between colloidal particles in NLCs near one wall and in an NLC cell

<sup>\*</sup>[cxwu@xmu.edu.cn](mailto:cxwu@xmu.edu.cn)

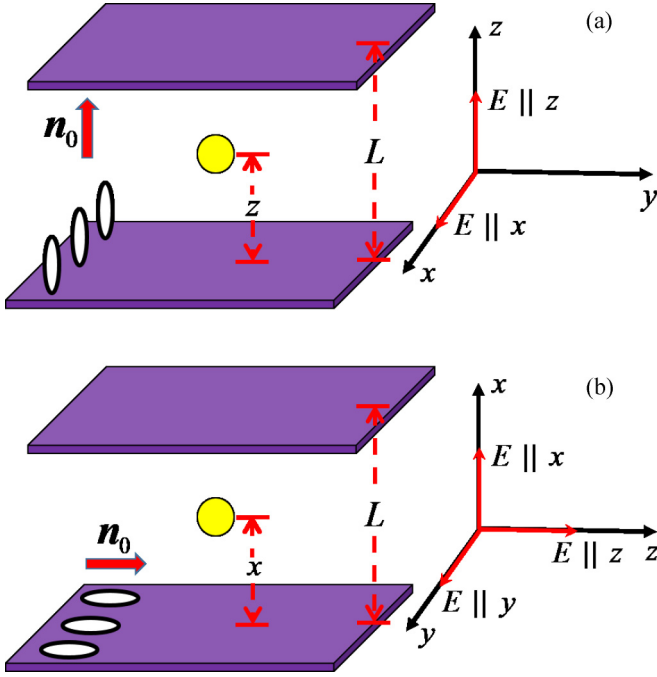


FIG. 1. Sketch of a microparticle suspended in a nematic cell with (a) homeotropic anchoring and (b) planar anchoring in the presence of an external field. The five cases of external fields applied are shown by red arrows in the two coordinate frames.

with or without an external field [47–49]. In the liquid crystal-particle coexisting system, it is found that an external field applied is able to drive particles apart [18], rotation [23], and realignment [50] and even trigger a positional transition [51], which can be used to manipulate the suspended microparticle. Despite the fact that the interaction of two particles and the particle-wall interaction for the particle-LC cell systems have been widely studied either via experimental or theoretical approaches [48,52,53], the properties of a single particle in such an NLC cell in the presence of an external electric field have not been fully theoretically addressed, partly due to the difficulties in mathematics involved in analyzing such kind of confined systems. However, it is of crucial importance to investigate, analytically if possible, the single microparticle-suspended NLC cell if one wants to find the corresponding applications of such kind of manipulations as demonstrated in experiments.

## II. THEORETICAL MODELING

We begin our investigation by considering a system of a spherical microparticle of radius  $r$  suspended in a NLC cell with  $L$ -thick spacers in the presence of an external electric field. For simplicity, the polarization of the microparticle is neglected compared to the influence of external field on the realignment of liquid crystal molecules. Figure 1 schematically illustrates two systems under an external field respectively with (a) a homeotropic anchoring and (b) a homogeneous planar anchoring at the two cell walls. The suspended microparticle induces a director distortion from the undeformed director field  $\mathbf{n}_0 = (0, 0, 1)$ , expressed by a two-component deviation field  $n_\mu$  ( $\mu = x, y$ ), both small at regions far away

from the microparticle. Here we deliberately use two different coordinate frames, as shown in Figs. 1(a) and 1(b), so that the same set of symbol subscripts [ $n_\mu$  ( $\mu = x, y$ )] can be usable under approximations for the two surface anchoring conditions throughout this paper. Assuming  $\mathbf{n} \approx (n_x, n_y, 1)$  with one Frank constant approximation, the effective elastic energy for the system reads [49]

$$U_e = K \int d^3x \left[ \frac{(\nabla n_\mu)^2}{2} - \frac{k^2}{2} (\mathbf{e} \cdot \mathbf{n})^2 - 4\pi P(\mathbf{x}) \partial_\mu n_\mu - 4\pi C(\mathbf{x}) \partial_z \partial_\mu n_\mu \right], \quad (1)$$

where  $K$  is the Frank constant;  $n_\mu$  ( $\mu = x, y$ ) represents the components of the director field  $\mathbf{n}$  perpendicular to  $\mathbf{n}_0$ ;  $P(\mathbf{x})$  and  $C(\mathbf{x})$  denote the dipole- and the quadrupole moment densities as functions of position  $\mathbf{x}$ , respectively; and  $k^2 = (4\pi K)^{-1} \Delta \varepsilon E^2$  with  $\Delta \varepsilon = \varepsilon_{\parallel} - \varepsilon_{\perp}$  the dielectric anisotropy of the NLC, which can be positive or negative with both cases considered in this paper. Here  $\varepsilon_{\parallel}$  and  $\varepsilon_{\perp}$  are the dielectric susceptibilities of the liquid crystal molecule parallel and perpendicular to the molecular long axis, respectively. For homeotropic anchoring, when an electric field is applied along the  $z$  axis [Fig. 1(a)], the Euler-Lagrange equations are given by [49]

$$\Delta n_\mu - k^2 n_\mu = 4\pi [\partial_\mu P(\mathbf{x}) - \partial_z \partial_\mu C(\mathbf{x})]. \quad (2)$$

On the other hand, for planar (homogeneous) anchoring, as shown in Fig. 1(b), when an external electric field is applied parallel to the  $x$  axis, we have the Euler-Lagrange equations written as [49]

$$\Delta n_\mu + k^2 \delta_{x\mu} n_\mu = 4\pi [\partial_\mu P(\mathbf{x}) - \partial_z \partial_\mu C(\mathbf{x})]. \quad (3)$$

If the applied electric field is parallel to the  $y$  axis [Fig. 1(b)], then the Euler-Lagrange equations are [49]

$$\Delta n_\mu + k^2 \delta_{y\mu} n_\mu = 4\pi [\partial_\mu P(\mathbf{x}) - \partial_z \partial_\mu C(\mathbf{x})]. \quad (4)$$

With Dirichlet boundary conditions  $n_\mu(\mathbf{s}) = 0$  on the two walls, the solution to Euler-Lagrange equations can be written as [49]

$$n_\mu(\mathbf{x}) = \int_V d^3x' G_\mu(\mathbf{x}, \mathbf{x}') [-\partial'_\mu P(\mathbf{x}') + \partial'_\mu \partial'_z C(\mathbf{x}')], \quad (5)$$

where  $G_\mu$  is the Green's function for  $n_\mu$ . Please note that here  $\mu$  in the integral does not follow Einstein summation notation and only dipolar contribution  $P(\mathbf{x}')$  is considered in this paper.

## III. RESULTS AND DISCUSSIONS

Given the Green's functions and the total energies in the Appendix for five different cases, we can plot the energy profiles as a function of microparticle position for different electric fields. The occurrence of positional transition triggered by an external electric field shall also be discussed.

### A. Homeotropic boundary condition

#### 1. External field perpendicular to the two plates

Now we first consider an electric field applied perpendicular to the two plates of the NLC cell with homeotropic

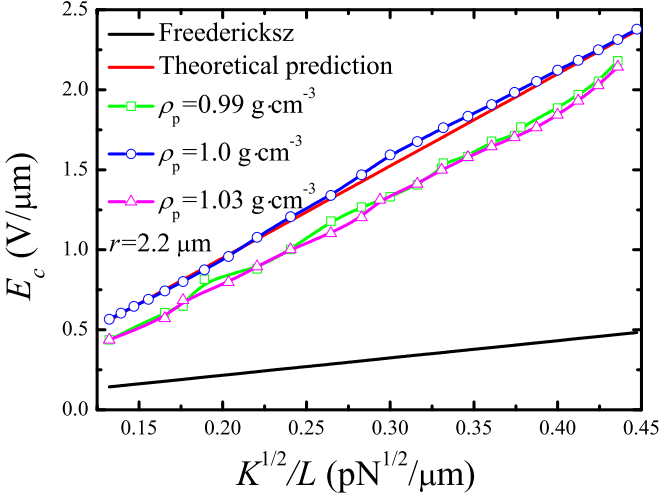


FIG. 2. Dependence of  $E_c$  and  $\sqrt{K}/L$  for different densities of microparticle (0.99, 1.0, and 1.03 g cm<sup>-3</sup>).

anchoring condition, i.e.,  $\mathbf{E}\parallel z$  in Fig. 1(a), and  $\Delta\varepsilon > 0$ , a Fréedericksz-like positional transition is found and the effects of cell thickness, Frank elastic constant, and microparticle size on the threshold value triggering the positional transition have been discussed in our previous paper [51]. Furthermore, in order to study the effect of microparticle density on the critical electric value, we plot the threshold value against  $\sqrt{K}/L$  for different microparticle densities (0.99, 1.0, and 1.03 g cm<sup>-3</sup>) in Fig. 2, where a Fréedericksz curve (black) is shown as well. It is clearly seen that the critical electric field for positional transition for different microparticle densities shows a Fréedericksz-like behavior, exhibiting straight lines nearly parallel to each other yet with a different slope from the Fréedericksz transition curve (black). A further calculation shows that such a Fréedericksz-like linear master curve of critical electric field does not depend or negligibly depend on the density of the microparticle, and the proposed formula for the critical electric field in Ref. [51] gives a prefactor of  $3\sqrt{\pi}$  in comparison with the Fréedericksz transition threshold expression. In the case when  $\Delta\varepsilon < 0$ , it is found that the microparticle is trapped at the midplane of the NLC cell, indicating that an application of external electric field does not trigger a positional phase transition. This is because when  $\mathbf{E}\parallel z$  and  $\Delta\varepsilon < 0$ , the realignment of liquid crystal molecules with the increase of the electric field narrows down the interaction potential well rather than flatten it, which creates a force directing toward the midplane much larger than the gravitational contribution and thus denies any positional transition.

### 2. External field parallel to the two plates

In the case when the external field is parallel to the two plates, i.e.,  $\mathbf{E}\parallel x$  in Fig. 1(a), surprisingly, the microparticle is trapped in the midplane of the NLC cell regardless of the sign of the molecular dielectric anisotropy, indicating that an application of external electric field, however large it is, cannot trigger a positional transition. This can be understood by considering the fact that the molecular long (short) axes tend to align along the direction of applied electric field as  $\Delta\varepsilon > 0$  ( $\Delta\varepsilon < 0$ ). As we increase the field applied, the

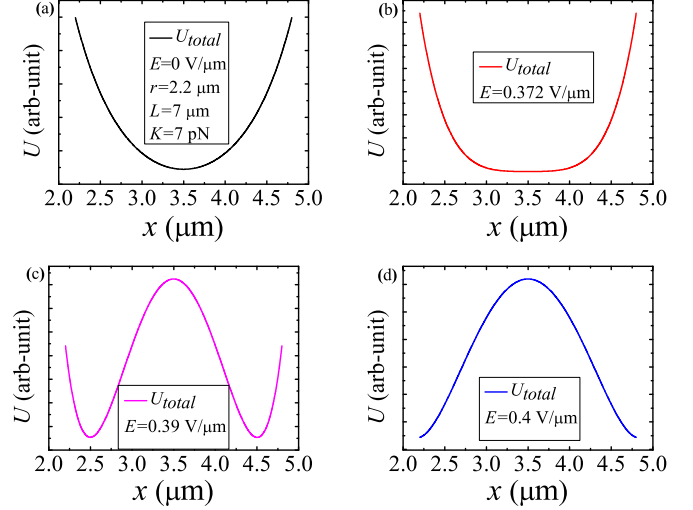


FIG. 3. Total energy profile as a function of the suspended microparticle position for an NLC cell with planar anchoring in the presence of different electric fields perpendicular to the two plates.

interaction potential is found to be narrowed down, corresponding to a strong midplane-directing restoring force. Therefore, for the homeotropic boundary condition, the positional transition occurs only in an NLC cell with positive molecular dielectric anisotropy when the external electric field is applied along the undeformed director field.

## B. Planar boundary condition

### 1. External field perpendicular to the two plates

When LC molecules are horizontally anchored on the two cell walls, as depicted in Fig. 1(b), let us first consider a positive dielectric anisotropy case  $\Delta\varepsilon > 0$  when an electric field is applied vertically to the two plates, i.e., along  $x$  axis in the figure. Intriguingly, a significant feature is observed regarding the profile of total energy as a function of microparticle position for four different electric fields, as illustrated in Fig. 3. In the presence of small field (below the critical electric value), Figs. 3(a) and 3(b) show that the interaction potential well around the midplane tends to be flattened in this region due to the realignment of liquid crystal molecules made by the increment of external electric field. However, when the electric field rises beyond the threshold value, there exists two symmetric equilibrium positions for the suspended microparticle [see Figs. 3(c) and 3(d)]. Which one the microparticle shifts to is decided by the perturbation stemming from the asymmetric buoyant force, i.e., by the density difference between NLC and microparticle ( $\rho_{LC} - \rho_{mp}$ ). Notably, the total energy now is almost equal to the elastic energy due to the fact that the gravitational contribution is much smaller in contrast to the elastic one, generating the depths of the two local minima in Fig. 3(c) [and Fig. 3(d)] nearly equal to each other.

To probe the influence of cell thickness and Frank constant on the critical field value, we plot the equilibrium position of the suspended microparticle against the applied electric field for different cell thicknesses (8, 9, 10, and 11  $\mu\text{m}$ ) and Frank elastic constants (8, 9, 10, and 11 pN), as shown

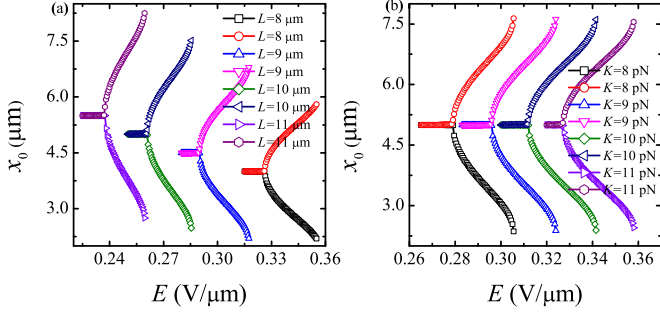


FIG. 4. Equilibrium position  $x_0$  in response to electric field for different (a) cell thicknesses (8, 9, 10, and 11  $\mu\text{m}$ ) with Frank elastic constant  $K = 7 \text{ pN}$  and the radius of microparticle  $r = 2.2 \mu\text{m}$ , and (b) Frank elastic constants (8, 9, 10, and 11  $\text{pN}$ ) with cell thickness  $L = 10 \mu\text{m}$  and radius of microparticle  $r = 2.2 \mu\text{m}$ .

in Figs. 4(a) and 4(b), where a positional transition occurs at some electric field threshold values and there exist two equilibrium positions when the external field applied exceeds the critical value. A more deeper investigation, as shown in Fig. 5, exhibits that the critical value of the external electric field is inversely proportional to  $L$  and linearly proportional to  $\sqrt{K}$ , a Fréedericksz-like behavior.

As a following step, we examine whether the critical electric value is correlated with the size and density of the microparticle. Surprisingly, Figs. 5(a) and 5(b) show that the plots of the equilibrium position of suspended microparticle against the applied electric field for different microparticle sizes and densities overlap each other, suggesting that the critical electric value is independent of or negligibly depends on microparticle size and density. To gain more insight into the dynamic behaviors of the microparticle, we

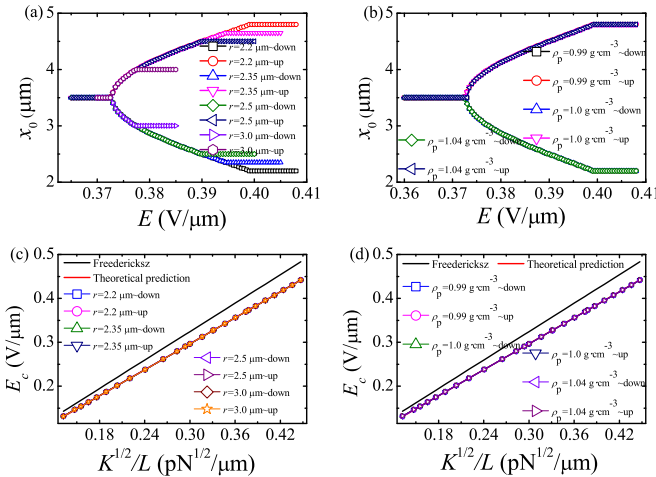


FIG. 5. Equilibrium position  $x_0$  for different (a) radii (2.2, 2.35, 2.5, and 3.0  $\mu\text{m}$ ) and (b) densities (0.99, 1.0, and 1.04  $\text{g cm}^{-3}$ ) of a microparticle with  $K = 7 \text{ pN}$  and  $L = 7 \mu\text{m}$ , showing the same critical value  $E_c$  of electric field triggering positional transition. The dependence of  $E_c$  on  $\sqrt{K}/L$  for different (c) radii (2.2, 2.35, 2.5, and 3.0  $\mu\text{m}$ ) and (d) densities (0.99, 1.0, and 1.04  $\text{g cm}^{-3}$ ) of the microparticle, obeying strictly a master curve which can be given by the theoretical prediction Eq. (6).

further plot the threshold value against  $\sqrt{K}/L$  in Figs. 5(c) and 5(d), where a Fréedericksz curve (black) is shown as well. It is interesting to find that the critical electric field to trigger a positional transition for a microparticle suspended in an NLC cell follows a Fréedericksz-like linear master curve with slightly different slopes, a universal one also valid for different microparticle sizes and densities.

By comparing the numerical calculation results with the Fréedericksz transition ( $\pi\sqrt{4\pi}/|\Delta\varepsilon|\sqrt{K}/L$ ) in Figs. 5(c) and 5(d), we found that the slope difference between them is by a prefactor of  $\sim 0.915$  and that enables us to propose a theoretical prediction for the critical electric field

$$E_c \simeq 0.915\mathcal{F}, \quad (6)$$

where  $\mathcal{F}$  denotes the Fréedericksz effect. Such a prediction, as shown by a straight line (red) in Figs. 5(c) and 5(d), agrees very well for different radii (2.2, 2.35, 2.5, and 3.0  $\mu\text{m}$ ) and densities (0.99, 1.0, and 1.04  $\text{g cm}^{-3}$ ) of microparticle. Due to the mathematical difficulty, we still do not know how to derive 0.915 analytically.

In the case when  $\Delta\varepsilon < 0$ , it is found that the suspended microparticle is trapped at the midplane of the NLC cell, which can be predicted by the profile change of the total energy potential well due to application of an external electric field in the vertical direction [ $x$  direction in Fig. 1(b)]. The short axes of liquid crystal molecules tend to align along the electric field, a result leading to the narrowing of total potential well and thereby generating strong restoring force acting on the suspended microparticle. Thus, in the case of a microparticle suspended in an NLC cell with planar anchoring condition in the presence of an external electric field applied perpendicular to the two plates, the positional transition triggered by the electric field may occur only under the condition of positive molecular dielectric anisotropy.

## 2. External field parallel to the two plates but perpendicular to the anchoring direction

Now let us consider the case when the electric field is applied parallel to the two plates but perpendicular to the anchoring direction, i.e., along  $y$  axis in Fig. 1(b). It is found that no matter  $\Delta\varepsilon > 0$  or  $\Delta\varepsilon < 0$ , the microparticle is always trapped at the midplane of the NLC cell regardless of the magnitude of the electric field applied, indicating that no positional transition occurs. The reason lies in that the realignment of the liquid crystal molecules in the presence of the external electric field does not flatten the interaction potential well substantially enough so as to decrease its corresponding equivalent restoring force on the microparticle to a small magnitude, with which the asymmetric gravitational force becomes competitive.

## 3. External field parallel to the two plates and the anchoring direction

Finally, we consider an NLC cell in the presence of an electric field parallel to the two plates and the anchoring direction as well, i.e.,  $\mathbf{E} \parallel \mathbf{z}$  in Fig. 1(b). If given a positive molecular dielectric anisotropy, namely  $\Delta\varepsilon > 0$ , then we can plot, as shown in Fig. 6, the total energy profile as a function of the suspended microparticle position for four chosen

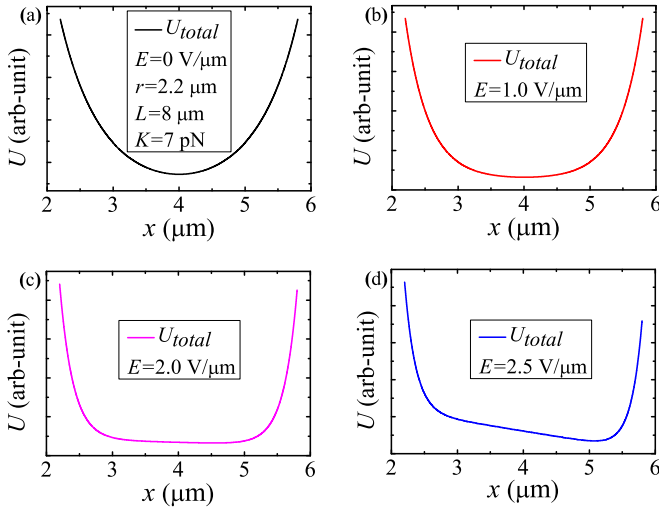


FIG. 6. Total energy profile as a function of the suspended microparticle position for an NLC cell with planar anchoring in the presence of four chosen electric fields parallel to the two plates and the anchoring direction as well.

electric fields. In the presence of a small external field, the total energy profile remains symmetric, indicating that the elastic interaction among LC molecules dominates the LC alignment, especially in the region close to the midplane. Thus the contribution made by asymmetric gravitational potential is trivial if compared with elasticity and the suspended microparticle will be trapped within its midplane, as demonstrated in Figs. 6(a) and 6(b). While as the electric field is increased, it is found that it tends to widen and flatten the bottom of the elastic potential well, which equivalently by contrast amplifies the relative contribution made by the asymmetric buoyant force to the total energy of the NLC cell. As a result, the buoyant force will drive the microparticle with ease from the midplane to a new equilibrium position [see Figs. 6(c) and 6(d)]. It is apparent that the sign of  $\rho_{LC} - \rho_{mp}$  determines the direction of the microparticle displacement. The bottom of the interaction potential well around the midplane is flattened due to the realignment of liquid crystal molecules made by the applied external field, which decreases the corresponding elastic restoring force built by the realignment. Once such a restoring force (corresponding to the elastic energy gradient) tuned by the external field in the cell is exceeded by the asymmetric buoyant force, it triggers a positional transition for the suspended microparticle from the midplane to its new equilibrium position.

In order to study the influence of cell thickness and Frank constant on the critical value of electric field, plots for the equilibrium position for the suspended microparticle against the applied electric field for different cell thicknesses (8, 10, 12, and 15  $\mu\text{m}$ ) and Frank elastic constants (8, 10, 12, and 15 pN) are presented in Figs. 7(a) and 7(b), where it is found that a positional transition occurs when the external field applied exceeds a threshold value. It is also shown that the thinner the cell thickness  $L$  is and the larger the Frank elastic constant  $K$  is, the larger the critical electric field is needed to trigger the positional transition.

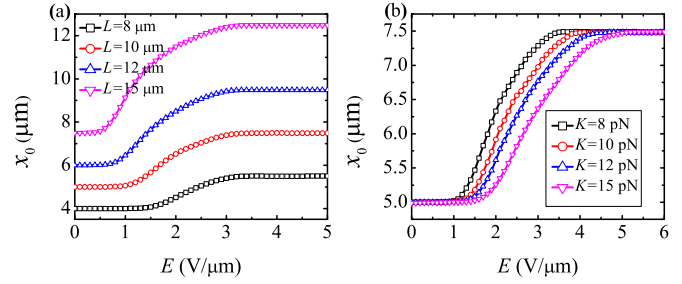


FIG. 7. Equilibrium position  $x_0$  in response to electric field for different (a) cell thicknesses (8, 10, 12, and 15  $\mu\text{m}$ ), where the Frank elastic constant and the radius of microparticle are set as  $K = 7$  pN and  $r = 2.5$   $\mu\text{m}$ , and (b) Frank elastic constants (8, 10, 12, and 15 pN), where the cell thickness and the radius of microparticle are set as  $L = 10$   $\mu\text{m}$  and  $r = 2.5$   $\mu\text{m}$ .

In a similar way to the previous sections, the dependence of the threshold value on microparticles size and density is also investigated. Figures 8(a) and 8(b) depict the equilibrium position against the applied electric field for different microparticle sizes and densities, where the overlapping of equilibrium position in Fig. 8(a) suggests that the critical electric value is almost independent of microparticle size. Whereas the symmetry of the equilibrium position of microparticle with density equal to  $0.99$   $\text{g cm}^{-3}$  and  $1.03$   $\text{g cm}^{-3}$  in Fig. 8(b) indicates that the slope of the master curve of critical electric value is nearly independent of the magnitude of equivalent microparticle density. To gain more insight into the dynamic behaviors of the microparticle, the threshold value is plotted against  $\sqrt{K}/L$  in Figs. 8(c) and 8(d), where a Fréedericksz transition curve (black) is shown as well. The existence of slight difference instead of overlapping each other for the equilibrium position of microparticle with density equal to

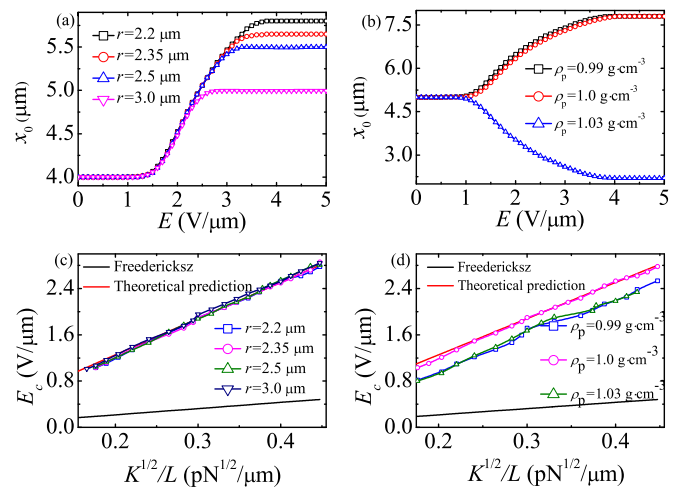


FIG. 8. (a) Equilibrium position  $x_0$  for different radii of microparticle with  $K = 7$  pN and  $L = 8$   $\mu\text{m}$ , showing the same critical value  $E_c$  of electric field triggering positional transition. (b)  $K = 8$  pN and  $L = 10$   $\mu\text{m}$ . The dependence of  $E_c$  and  $\sqrt{K}/L$  for different (c) radii (2.2, 2.35, 2.5, and 3.0  $\mu\text{m}$ ) and (d) densities (0.99, 1.0, and 1.03  $\text{g cm}^{-3}$ ) of microparticle, obeying strictly a master curve given by theoretical prediction Eq. (7).

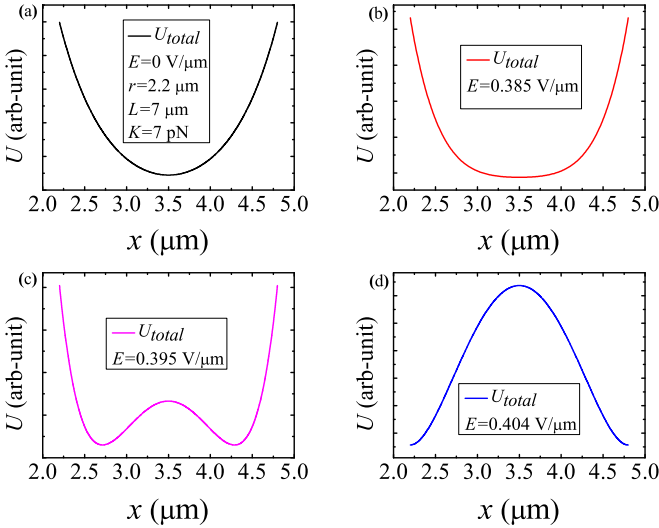


FIG. 9. Total energy profile as a function of the suspended microparticle position for different external electric fields.

$0.99 \text{ g cm}^{-3}$  and  $1.0 \text{ g cm}^{-3}$  in Fig. 8(b) leads to different intercepts of the Fréedericksz-like linear master curves for critical electric field in Fig. 8(d). Further study of electric field threshold shows that it seems to be inversely proportional to cell thickness  $L$  and proportional to the root square of the Frank elastic constant  $K$ , a behavior similar to the field threshold of Fréedericksz phase transition. As before, the critical electric field for a positional transition to occur for a microparticle suspended in a NLC cell remains unchanged for different microparticle sizes and densities.

Similarly, a contrast between the numerical calculation results and the traditional Fréedericksz transition curve ( $\pi\sqrt{4\pi/|\Delta\varepsilon|}\sqrt{K}/L$ ) in Figs. 8(c) and 8(d) shows that the slope difference between them is by a prefactor of  $\sim 5.8$ . More specifically, an explicit expression

$$E_c \simeq 5.8\mathcal{F} - 0.08 = 5.8\pi\sqrt{\frac{4\pi K}{|\Delta\varepsilon|L^2}} - 0.08 \quad (7)$$

for critical electric field can be proposed as a theoretical prediction. Such a prediction, as shown by straight line (red) in Figs. 8(c) and 8(d), agrees very well for different radii (2.2, 2.35, 2.5, and  $3.0 \mu\text{m}$ ) and densities (0.99, 1.0, and  $1.03 \text{ g cm}^{-3}$ ) of microparticle. This once again verifies the conclusion that the critical electric field is independent of microparticle size, of which the reason might lie in that in the present theoretical model, the microparticle is approximately treated as a dipole in the far-field expansion.

As for the case  $\Delta\varepsilon < 0$  when the external field applied parallel to both the two plates and the anchoring direction, i.e.,  $\mathbf{E}\parallel\mathbf{z}$  in Fig. 1(b), a bistable equilibrium state structure is found as the electric field exceeds a threshold value, as illustrated in Fig. 9. In the small-field region, the external field applied tends to, first, flatten the bottom of potential well, as shown in Figs. 9(a) and 9(b). Further increase of external field will change the one-state potential structure to a bistable one. As the gravitational contribution to the total energy is still negligibly small compared to the elastic one, one sees no

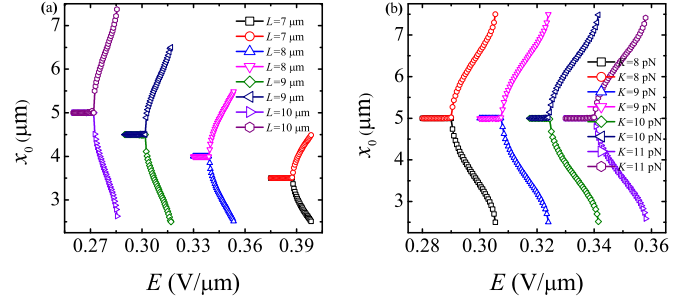


FIG. 10. Equilibrium position  $x_0$  in response to electric field for different (a) cell thicknesses (7, 8, 9, and  $10 \mu\text{m}$ ), where the Frank elastic constant and the radius of microparticle are set as  $K = 7 \text{ pN}$  and  $r = 2.5 \mu\text{m}$ , and (b) Frank elastic constants (8, 9, 10, and  $11 \text{ pN}$ ), where the cell thickness and the radius of microparticle are set as  $L = 10 \mu\text{m}$  and  $r = 2.5 \mu\text{m}$ .

involvement of gravitational force to the determination of the critical value of positional transition for the microparticle in the NLC cell. Thus, the positional transition in this case does not come from the competition between the gravitational force and the equivalent elastic force but rather purely from the bistable local minimum of the elastic potential, as shown in Figs. 9(c) and 9(d). Nevertheless the asymmetric gravitational force still plays a very important role in determining the direction of microparticle motion (up or down) by acting as a small but significant perturbation, or more precisely, by the sign of buoyant force (the sign of  $\rho_{\text{LC}} - \rho_{\text{mp}}$ ). Therefore, the magnitude of the asymmetric gravitational force in this case is trivial but not its sign.

In order to understand how cell thickness and Frank elastic constant affect the critical value of electric field, we plot equilibrium position against the applied electric field for different cell thicknesses (7, 8, 9, and  $10 \mu\text{m}$ ) and Frank elastic constants (8, 9, 10, and  $11 \text{ pN}$ ), as shown in Figs. 10(a) and 10(b), where a bifurcation of equilibrium position is found due to the bistable state structure of elastic potential and a positional transition occurs when the external field applied reaches a threshold value.

Finally, in order to gain more insights into the physics hidden behind the dynamic behaviors of microparticle, it is worthwhile to evaluate whether the critical electric value is correlated with the size and density of the microparticle. The dependence of the equilibrium position on the applied electric field for different microparticle sizes and densities is shown in Figs. 11(a) and 11(b), where the strict overlapping of equilibrium position in the figures implies that the critical electric value is, as shown in the previous section, independent of microparticle size and density. For a better understanding of the dynamic behaviors of the microparticle, we further plot the threshold value against  $\sqrt{K}/L$  in Figs. 11(c) and 11(d), with a Fréedericksz transition curve (black) shown as well. It is found that the critical electric field triggering a positional transition for a microparticle suspended in a NLC cell follows a Fréedericksz master curve irrelevant to microparticle size and density.

More precisely, by comparing the numerical calculation results with the Fréedericksz effect curve ( $\pi\sqrt{4\pi/|\Delta\varepsilon|}\sqrt{K}/L$ ) in Figs. 11(c) and 11(d), it is found that the slope difference

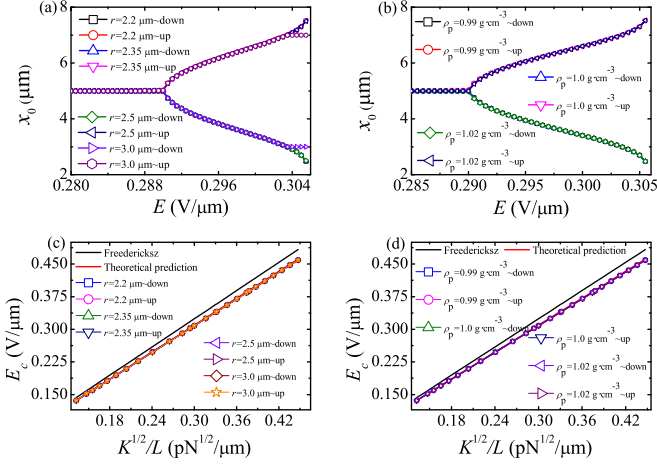


FIG. 11. Equilibrium position  $x_0$  for different (a) radii (2.2, 2.35, 2.5, and  $3.0 \mu\text{m}$ ); (b) densities ( $0.99, 1.0$ , and  $1.02 \text{ g cm}^{-3}$ ) of microparticle with  $K = 8 \text{ pN}$  and  $L = 10 \mu\text{m}$ , showing the same critical value  $E_c$  of electric field triggering positional transition. The dependence of  $E_c$  and  $\sqrt{K}/L$  for different (c) radii (2.2, 2.35, 2.5, and  $3.0 \mu\text{m}$ ) and (d) densities ( $0.99, 1.0$ , and  $1.02 \text{ g cm}^{-3}$ ) of microparticle, obeying strictly a master curve given by theoretical prediction Eq. (8).

between them is by a prefactor of  $\sim 3/\pi$ , leading to a proposed theoretical prediction

$$E_c \simeq \frac{3}{\pi} \mathcal{F} = 6 \sqrt{\frac{\pi K}{|\Delta\varepsilon| L^2}} \quad (8)$$

for the critical electric field. Such a prediction, as shown by the straight line (red) in Figs. 11(c) and 11(d), agrees very well for different radii (2.2, 2.35, 2.5, and  $3.0 \mu\text{m}$ ) and densities ( $0.99, 1.0$ , and  $1.02 \text{ g cm}^{-3}$ ) of microparticle.

Based on the discussions in the sections above, it is quite obvious that the external electric field applied enhances the existing anisotropy of distortion generated by the boundaries of the NLC cell shaped by the the movable suspended microparticle and the two parallel walls. The LC molecules surrounding the suspended microparticle together with the boundary conditions create a potential trap for the microparticle, with its depth and width tuned by the external field applied. The net restoring force on the microparticle along

the vertical direction, which is determined by the gradient of the potential well, becomes tunable by the external field. Due to the steepness of the potential well near the midplane in the absence of external field, such a net force is usually very large in comparison with the gravitational force of the microparticle and thus traps the microparticle in the midplane of the NLC cell. However, there exists a possibility that the gravitational force can come into play when the external field applied reaches a critical value, triggering the motion of the microparticle, which proved to be a positional transition [51]. It looks like that the electric field threshold is a signal to realign the surrounding LC molecules to such an extent that a fast track is constructed along the vertical direction, enabling the sudden motion of the microparticle driven by the gravitational force. After a thorough discussion on such a translational transition in a microparticle-suspended NLC cell in the presence of an external electric field, we come up with a table of all the conditions combined for a positional transition to occur in such a system, as shown in Table I. It is found in the Table that of the 10 combinations of field direction, molecular dielectric anisotropy, and anchoring feature, only 4 combinations demonstrate the possible occurrence of positional transition. Moreover, for a nematic liquid crystal cell with planar surface alignment, a bistable equilibrium structure for the transition is found when the direction of applied electric field is (a) perpendicular to the two plates of the cell with positive molecular dielectric anisotropy or (b) parallel to both the two plates and the anchoring direction of the cell with negative molecular dielectric anisotropy.

#### IV. CONCLUSION

In summary, using the Green's function method, the total energy for a microparticle suspended in an NLC cell in the presence of an external electric field is calculated. The external electric field applied, which has been widely accepted to be able to realign LC molecules surrounding the microparticle, can be used to tune the position of the microparticle in the cell. It is found that the vertical translational motion from the midplane to a new equilibrium position is triggered by a threshold value of electric field tuning (decreasing) the net restoring force so as to let the gravitational force come into play. The new equilibrium position is decided via a competition between the buoyant (gravitational) force and the

TABLE I. Combined conditions for positional transition to occur (+) and not to occur (−) for a microparticle suspended in an NLC cell in the presence of an external electric field.

Anchoring	Molecular dielectric anisotropy	Field direction	
		$\mathbf{E} \perp$ plates	$\mathbf{E} \parallel$ plates
Homeotropic	$\Delta\varepsilon > 0$	+	—
	$\Delta\varepsilon < 0$	—	—
Planar	$\Delta\varepsilon > 0$	+/bistable	$\mathbf{E} \perp$ anchoring —
	$\Delta\varepsilon < 0$	—	$\mathbf{E} \parallel$ anchoring +
			+/bistable

effective force built on the microparticle. The threshold value of external field, which triggers positional transition under appropriate combined conditions of surface anchoring feature, field direction and molecular dielectric anisotropy, depends on thickness  $L$  and Frank elastic constant  $K$  and slightly on the microparticle size and density, in a Fréedericksz-like manner as coined by the authors before, but by a factor. For an NLC cell with planar surface alignment, a bistable equilibrium structure for the transition is found when the direction of the applied electric field is (a) perpendicular to the cell wall with positive molecular dielectric anisotropy or (b) parallel to the undeformed director field  $\mathbf{n}_0$  of the NLC cell with negative molecular dielectric anisotropy. Except for the positional transition, when the electric field applied is parallel to the two plates and perpendicular to the anchoring direction, the microparticle suspended in NLC will be trapped in the midplane, regardless of the sign of the molecular dielectric anisotropy. Explicit formulas proposed for the critical electric field agrees extremely well with the numerical calculation.

### ACKNOWLEDGMENTS

This work was funded by the National Science Foundation of China under Grants No. 11974292, No.11974291, and No. 11947401.

### APPENDIX: GREEN'S FUNCTIONS AND TOTAL ENERGIES

#### 1. Homeotropic boundary condition

Here we first consider an NLC cell sandwiched between two parallel plates, where LC molecules are homeotropically anchored and the coordinate  $z$  axis is chosen along the normal direction of the two plates, as shown in Fig. 1(a).

##### a. External field perpendicular to the two plates

In this case, when an electric field is applied perpendicular to the two plates, i.e.,  $\mathbf{E}\parallel z$  in Fig. 1(a), the corresponding Euler-Lagrange equations are written as Eq. (2). With Dirichlet boundary conditions  $n_\mu(z=0) = n_\mu(z=L) = 0$ , the Green's function can be derived as [49]

$$G_\mu(\mathbf{x}, \mathbf{x}') = \frac{4}{L} \sum_{n=1}^{\infty} \sum_{m=-\infty}^{\infty} e^{im(\varphi-\varphi')} \sin \frac{n\pi z}{L} \times \sin \frac{n\pi z'}{L} I_m(\lambda_n \rho_{<}) K_m(\lambda_n \rho_{>}), \quad (\text{A1})$$

where  $\varphi$  and  $\varphi'$  are the azimuthal angles,  $z$  and  $z'$  are the positional coordinates,  $I_m$  and  $K_m$  are modified Bessel functions,  $\rho_{<}$  is the smaller one between  $\sqrt{x^2 + y^2}$  and  $\sqrt{x'^2 + y'^2}$ , and  $\lambda_n = [(n\pi/L)^2 + \Delta\epsilon E^2/4\pi K]^{1/2}$  with  $L$  the thickness of the NLC cell. Using the definition of self-energy given in terms of Green's function [49],

$$U_{dd}^{\text{self}} = -2\pi K p^2 \partial_\mu \partial'_\mu H_\mu(\mathbf{x}, \mathbf{x}')|_{\mathbf{x}=\mathbf{x}'}, \quad (\text{A2})$$

where  $H_\mu(\mathbf{x}, \mathbf{x}') = G_\mu(\mathbf{x}, \mathbf{x}') - 1/|\mathbf{x} - \mathbf{x}'|$ , we obtain the elastic energy  $U_e^I$  for a microparticle suspended in an NLC cell in the presence of an electric field. Besides the elastic energy, the gravitational potential  $U_g$  due to buoyant force should be

considered as well, leading to a total energy written as

$$U_{\text{total}}^I = U_e^I + U_g = -2\pi K p^2 \left[ -\frac{4}{L} \sum_{n=1}^{\infty} \lambda_n^2 \sin^2 \left( \frac{n\pi z}{L} \right) K_0(\lambda_n \rho) + \frac{1}{\rho^3} \right]_{\rho \rightarrow 0} - \frac{4}{3} \pi r^3 (\rho_{\text{LC}} - \rho_{\text{mp}}) g z, \quad (\text{A3})$$

where  $r$  is the radius of microparticle,  $p = 2.04r^2$  is the magnitude of the equivalent dipole moment for  $P(\mathbf{x}')$  in Eq. (5), as in the previous literature [3,47–49],  $\rho_{\text{LC}} - \rho_{\text{mp}}$  is the density difference between liquid crystal and microparticle, and  $g = 9.8 \text{ m/s}^2$  is the gravitational acceleration.

##### b. External field parallel to the two plates

For the case of an electric field parallel to the two plates, i.e.,  $\mathbf{E}\parallel x$  in Fig. 1(a), the Euler-Lagrange equations for  $n_x$  and  $n_y$  are written as Eq. (3). With Dirichlet boundary conditions  $n_\mu(z=0) = n_\mu(z=L) = 0$ , the related Green's functions  $G_x$  and  $G_y$  are given by

$$G_x(\mathbf{x}, \mathbf{x}') = \frac{4}{L} \sum_{n=1}^{\infty} \sum_{m=-\infty}^{\infty} e^{im(\varphi-\varphi')} \sin \frac{n\pi z}{L} \times \sin \frac{n\pi z'}{L} I_m(\nu_n \rho_{<}) K_m(\nu_n \rho_{>}),$$

$$G_y(\mathbf{x}, \mathbf{x}') = \frac{4}{L} \sum_{n=1}^{\infty} \sum_{m=-\infty}^{\infty} e^{im(\varphi-\varphi')} \sin \frac{n\pi z}{L} \times \sin \frac{n\pi z'}{L} I_m(\mu_n \rho_{<}) K_m(\mu_n \rho_{>}), \quad (\text{A4})$$

where  $\nu_n = [(n\pi/L)^2 - \Delta\epsilon E^2/4\pi K]^{1/2}$  and  $\mu_n = n\pi/L$ . Analogously to the previous case, we can obtain the elastic energy  $U_e^{\text{II}}$  and the total energy  $U_{\text{total}}^{\text{II}}$  is written as

$$U_{\text{total}}^{\text{II}} = U_e^{\text{II}} + U_g = -2\pi K p^2 \left[ -\frac{2}{L} \sum_{n=1}^{\infty} \sin^2 \left( \frac{n\pi z}{L} \right) (\alpha_n + \beta_n) + \frac{1}{\rho^3} \right]_{\rho \rightarrow 0} - \frac{4}{3} \pi r^3 (\rho_{\text{LC}} - \rho_{\text{mp}}) g z, \quad (\text{A5})$$

where  $\alpha_n = \nu_n^2 K_0(\nu_n \rho) + \mu_n^2 K_0(\mu_n \rho)$  and  $\beta_n = \nu_n^2 K_2(\nu_n \rho) - \mu_n^2 K_2(\mu_n \rho)$ .

### 2. Planar boundary condition

#### a. External field perpendicular to the two plates

When an electric field is applied vertically to the two plates, i.e.,  $\mathbf{E}\parallel x$  in Fig. 1(b), the Euler-Lagrange equations are given by Eq. (3), and the corresponding Green's functions  $G_x$  and  $G_y$  read as [49]

$$G_x(\mathbf{x}, \mathbf{x}') = \frac{4}{L} \sum_{n=1}^{\infty} \sum_{m=-\infty}^{\infty} e^{im(\varphi-\varphi')} \sin \frac{n\pi x}{L} \times \sin \frac{n\pi x'}{L} I_m(\nu_n \rho_{<}) K_m(\nu_n \rho_{>}),$$



$$G_y(\mathbf{x}, \mathbf{x}') = \frac{4}{L} \sum_{n=1}^{\infty} \sum_{m=-\infty}^{\infty} e^{im(\varphi-\varphi')} \sin \frac{n\pi x}{L} \times \sin \frac{n\pi x'}{L} I_m(\mu_n \rho_{<}) K_m(\mu_n \rho_{>}), \quad (\text{A6})$$

with  $v_n$  and  $\mu_n$  identical to those in Eq. (A4). Similarly, the elastic energy  $U_e^{\text{III}}$  can be obtained and the total energy  $U_{\text{total}}^{\text{III}}$  can be derived as

$$U_{\text{total}}^{\text{III}} = U_e^{\text{III}} + U_g = -2\pi K p^2 \left( \frac{4}{L} \sum_{n=1}^{\infty} \mu_n^2 \left\{ \cos^2 \left( \frac{n\pi x}{L} \right) K_0(v_n \rho) - \frac{1}{2} \times \sin^2 \left( \frac{n\pi x}{L} \right) [K_0(\mu_n \rho) - K_2(\mu_n \rho)] \right\} + \frac{1}{\rho^3} \right)_{\rho \rightarrow 0} - \frac{4}{3} \pi r^3 (\rho_{\text{LC}} - \rho_{\text{mp}}) g x, \quad (\text{A7})$$

where  $x$  denotes the vertical position of the microparticle.

#### b. External field parallel to the two plates but perpendicular to the anchoring direction

When the electric field applied is parallel to the two plates but perpendicular to the anchoring direction, i.e.,  $\mathbf{E} \parallel y$  in Fig. 1(b), the Euler-Lagrange equations can be given by Eq. (4), with their corresponding Green's functions  $G_x$  and  $G_y$  written as

$$G_x(\mathbf{x}, \mathbf{x}') = \frac{4}{L} \sum_{n=1}^{\infty} \sum_{m=-\infty}^{\infty} e^{im(\varphi-\varphi')} \sin \frac{n\pi x}{L} \times \sin \frac{n\pi x'}{L} I_m(\mu_n \rho_{<}) K_m(\mu_n \rho_{>}),$$

$$G_y(\mathbf{x}, \mathbf{x}') = \frac{4}{L} \sum_{n=1}^{\infty} \sum_{m=-\infty}^{\infty} e^{im(\varphi-\varphi')} \sin \frac{n\pi x}{L} \times \sin \frac{n\pi x'}{L} I_m(v_n \rho_{<}) K_m(v_n \rho_{>}), \quad (\text{A8})$$

with the same  $v_n$  and  $\mu_n$  as those in Eq. (A6). In a similar way, the total energy  $U_{\text{total}}^{\text{IV}}$  is given by

$$U_{\text{total}}^{\text{IV}} = U_e^{\text{IV}} + U_g = -2\pi K p^2 \left\{ \frac{4}{L} \sum_{n=1}^{\infty} \mu_n^2 \cos^2 \left( \frac{n\pi x}{L} \right) K_0(\mu_n \rho) - \frac{2}{L} \sum_{n=1}^{\infty} v_n^2 \sin^2 \left( \frac{n\pi x}{L} \right) [K_0(v_n \rho) - K_2(v_n \rho)] + \frac{1}{\rho^3} \right\}_{\rho \rightarrow 0} - \frac{4}{3} \pi r^3 (\rho_{\text{LC}} - \rho_{\text{mp}}) g x, \quad (\text{A9})$$

where  $U_e^{\text{IV}}$  is the elastic energy.

#### c. External field parallel to the two plates and the anchoring direction

Finally, if an electric field is applied parallel to the two plates and the planar anchoring direction as well, i.e.,  $\mathbf{E} \parallel z$  in Fig. 1(b). Given the corresponding Euler-Lagrange equations Eq. (2), the Green's functions are [49]

$$G_\mu(\mathbf{x}, \mathbf{x}') = \frac{4}{L} \sum_{n=1}^{\infty} \sum_{m=-\infty}^{\infty} e^{im(\varphi-\varphi')} \sin \frac{n\pi x}{L} \times \sin \frac{n\pi x'}{L} I_m(\lambda_n \rho_{<}) K_m(\lambda_n \rho_{>}), \quad (\text{A10})$$

with the same  $\lambda_n$  as that in Eq. (A1). Similarly, the total energy  $U_{\text{total}}^{\text{V}}$  can be derived as

$$U_{\text{total}}^{\text{V}} = U_e^{\text{V}} + U_g = -2\pi K p^2 \left\{ \frac{4}{L} \sum_{n=1}^{\infty} \left( \frac{n\pi}{L} \right)^2 \cos^2 \left( \frac{n\pi x}{L} \right) K_0(\lambda_n \rho) - \frac{2}{L} \sum_{n=1}^{\infty} \lambda_n^2 \sin^2 \left( \frac{n\pi x}{L} \right) [K_0(\lambda_n \rho) - K_2(\lambda_n \rho)] + \frac{1}{\rho^3} \right\}_{\rho \rightarrow 0} - \frac{4}{3} \pi r^3 (\rho_{\text{LC}} - \rho_{\text{mp}}) g x, \quad (\text{A11})$$

with  $U_e^{\text{V}}$  the elastic energy.

- 
- [1] P. Poulin, H. Stark, T. C. Lubensky, and D. A. Weitz, *Science* **275**, 1770 (1997).
- [2] P. Poulin and D. A. Weitz, *Phys. Rev. E* **57**, 626 (1998).
- [3] T. C. Lubensky, D. Petey, N. Currier, and H. Stark, *Phys. Rev. E* **57**, 610 (1998).
- [4] C. P. Lapointe, T. G. Mason, and I. I. Smalyukh, *Science* **326**, 1083 (2009).
- [5] H. Stark, *Phys. Rep.* **351**, 387 (2001).
- [6] H. Stark, *Phys. Rev. E* **66**, 032701 (2002).
- [7] Y. Wang, P. Zhang, and J. Z. Y. Chen, *Phys. Rev. E* **96**, 042702 (2017).
- [8] X. Yao, H. Zhang, and J. Z. Y. Chen, *Phys. Rev. E* **97**, 052707 (2018).
- [9] B. Senyuk, O. Puls, O. M. Tovkach, S. B. Chernyshuk, and I. I. Smalyukh, *Nat. Commun.* **7**, 10659 (2016).
- [10] Y. Zhou, B. Senyuk, R. Zhang, I. I. Smalyukh, and J. J. de Pablo, *Nat. Commun.* **10**, 1000 (2019).
- [11] B. Comiskey, J. Albert, H. Yoshizawa, and J. Jacobson, *Nature* **394**, 253 (1998).
- [12] Z. Wang and J. Zhe, *Chip* **11**, 1280 (2011).
- [13] T. Araki, M. Buscaglia, T. Bellini, and H. Tanaka, *Nat. Mater.* **10**, 303 (2011).
- [14] I. I. Smalyukh, *Annu. Rev. Condens. Matter Phys.* **9**, 207 (2018).
- [15] Y.-K. Kim, X. Wang, P. Mondkar, E. Bokusoglu, and N. Abbott, *Nature* **557**, 539 (2018).
- [16] E. A. Nance, G. F. Woodworth, K. A. Sailor, T.-Y. Shih, Q. Xu, G. Swaminathan, D. Xiang, C. Eberhart, and J. Hanes, *Sci. Trans. Med.* **4**, 149ra119 (2012).
- [17] S. J. Woltman, G. D. Jay, and G. P. Crawford, *Nat. Mater.* **6**, 929 (2007).

- [18] P. Poulin, V. Cabuil, and D. A. Weitz, *Phys. Rev. Lett.* **79**, 4862 (1997).
- [19] M. Vilfan, N. Osterman, M. Čopič, M. Ravnik, S. Žumer, J. Kotar, D. Babič, and I. Poberaj, *Phys. Rev. Lett.* **101**, 237801 (2008).
- [20] U. Ognysta, A. Nych, V. Nazarenko, I. Muševič, M. Škarabot, M. Ravnik, S. Žumer, I. Poberaj, and D. Babič, *Phys. Rev. Lett.* **100**, 217803 (2008).
- [21] M. Škarabot, M. Ravnik, S. Žumer, U. Tkalec, I. Poberaj, D. Babič, N. Osterman, and I. Muševič, *Phys. Rev. E* **77**, 031705 (2008).
- [22] A. V. Ryzhkova, M. Škarabot, and I. Muševič, *Phys. Rev. E* **91**, 042505 (2015).
- [23] C. P. Lapointe, S. Hopkins, T. G. Mason, and I. I. Smalyukh, *Phys. Rev. Lett.* **105**, 178301 (2010).
- [24] U. M. Ognysta, A. B. Nych, V. A. Uzunova, V. M. Pergamenschik, V. G. Nazarenko, M. Škarabot, and I. Muševič, *Phys. Rev. E* **83**, 041709 (2011).
- [25] S.-J. Kim, B.-K. Lee, and J.-H. Kim, *Liq. Cryst.* **43**, 1589 (2016).
- [26] D. Andrienko, M. Tasinkevych, P. Patrício, M. P. Allen, and M. M. Teloda Gama, *Phys. Rev. E* **68**, 051702 (2003).
- [27] K. Izaki and Y. Kimura, *Phys. Rev. E* **87**, 062507 (2013).
- [28] T. Araki and J. Nagura, *Phys. Rev. E* **95**, 012706 (2017).
- [29] C. Conklin, O. M. Tovkach, J. Viñals, M. C. Calderer, D. Golovaty, O. D. Lavrentovich, and N. J. Walkington, *Phys. Rev. E* **98**, 022703 (2018).
- [30] F. L. Calderon, T. Stora, O. Mondain Monval, P. Poulin, and J. Bibette, *Phys. Rev. Lett.* **72**, 2959 (1994).
- [31] M. Yada, J. Yamamoto, and H. Yokoyama, *Phys. Rev. Lett.* **92**, 185501 (2004).
- [32] K. Takahashi, M. Ichikawa, and Y. Kimura, *Phys. Rev. E* **77**, 020703(R) (2008).
- [33] M. Škarabot, A. V. Ryzhkova, and I. Muševič, *J. Mol. Liq.* **267**, 384 (2018).
- [34] O. P. Pishnyak, S. Tang, J. R. Kelly, S. V. Shiyanovskii, and O. D. Lavrentovich, *Phys. Rev. Lett.* **99**, 127802 (2007).
- [35] O. P. Pishnyak, S. V. Shiyanovskii, and O. D. Lavrentovich, *J. Mol. Liq.* **164**, 132 (2011).
- [36] J. M. Pagès, J. Ignés-Mullol, and F. Sagués, *Phys. Rev. Lett.* **122**, 198001 (2019).
- [37] R. W. Ruhwandl and E. M. Terentjev, *Phys. Rev. E* **54**, 5204 (1996).
- [38] R. W. Ruhwandl and E. M. Terentjev, *Phys. Rev. E* **56**, 5561 (1997).
- [39] J. C. Loudet and P. Poulin, *Phys. Rev. Lett.* **87**, 165503 (2001).
- [40] N. Atzin, O. Guzmán, O. Gutiérrez, L. S. Hirst, and S. Ghosh, *Phys. Rev. E* **97**, 062704 (2018).
- [41] C. Denniston, E. Orlandini, and J. M. Yeomans, *Phys. Rev. E* **63**, 056702 (2001).
- [42] S. Changizrezaei and C. Denniston, *Phys. Rev. E* **99**, 052701 (2019).
- [43] M. Ravnik, and S. Žumer, *Liq. Cryst.* **36**, 1201 (2009).
- [44] M. Ravnik, *Liq. Cryst. Today* **20**, 77 (2011).
- [45] M. Tasinkevych, N. M. Silvestre, and M. M. T. da Gama, *New J. Phys.* **14**, 073030 (2012).
- [46] S. R. Seyednejad, M. R. Mozaffari, and M. R. Ejtehad, *Phys. Rev. E* **88**, 012508 (2013).
- [47] S. B. Chernyshuk and B. I. Lev, *Phys. Rev. E* **81**, 041701 (2010).
- [48] S. B. Chernyshuk and B. I. Lev, *Phys. Rev. E* **84**, 011707 (2011).
- [49] S. B. Chernyshuk, O. M. Tovkach, and B. I. Lev, *Phys. Rev. E* **85**, 011706 (2012).
- [50] G. D'Adamo, D. Marenduzzo, C. Micheletti, and E. Orlandini, *Phys. Rev. Lett.* **114**, 177801 (2015).
- [51] K. Xiao, X. Chen, and C. X. Wu, *Phys. Rev. Res.* **1**, 033041 (2019).
- [52] S.-J. Kim and J.-H. Kim, *Soft Matter* **10**, 2664 (2014).
- [53] B.-K. Lee, S.-J. Kim, B. Lev, and J.-H. Kim, *Phys. Rev. E* **95**, 012709 (2017).